FARADAY RESEARCH ARTICLE

Towards magnetic trapping of molecules

Bretislav Friedrich,*† Robert deCarvalho, Jinha Kim, David Patterson, Jonathan D. Weinstein and John M. Doyle*

Department of Physics, Lyman Laboratory, Harvard University, Cambridge, MA 02138, USA

The advent of buffer-gas loaded magnetic traps for atoms has opened the possibility of trapping paramagnetic molecules. We survey our results on the loading, trapping and spectroscopy of Eu atoms that demonstrated the technique. The principles governing molecular trapping considering in particular the O_2 and NO systems are outlined. The trapping of molecules should prove particularly useful in spectroscopy, especially ultra-high resolution spectroscopy that requires cold (slow), trapped (long interaction time) samples. Similar to cold atoms, cold molecules could be interrogated at a level of detail which is likely to provide new insights into their structure and interactions.

1 Introduction

Most of the effort in trapping of neutrals is currently limited to atoms whose structure allows for optical cooling.[1] A notable exception is atomic hydrogen which can be cooled by thermalization with liquid helium films.[2] So, despite the fact that many ground state atoms are paramagnetic (about 70% of the Periodic Table), only a few have been trapped. This paucity of trapped species has been due to the lack of a general cooling technique that would allow loading the atoms into a conservative trapping field.

Recently, we demonstrated that Eu and Cr atoms can be loaded into a magnetic trap using a cold He buffer gas.[3,4,5] This cooling technique is independent of the detailed structure of the trapped species. In particular, the combination of buffer gas loading with magnetic trapping should make paramagnetic atoms and paramagnetic molecules readily trappable. Table 1 lists paramagnetic ground-state atoms and their maximum magnetic dipole moments.

In this paper we discuss the potential applications of molecular trapping (Section 2), give details of buffer gas loading relevant to both atomic and molecular trapping (Section 3), describe magnetic trapping and spectrosocopy of Eu atoms (Section 4), and finally outline the theory of magnetic trapping of Hund's case (a) and (b) molecules as exemplified by O_2 and NO (Section 5).

2 Molecular trapping: potential applications

Trapping of molecules should prove particularly useful in spectrosocopy and the study of molecular structure,[8] especially in ultra-high resolution spectroscopy that requires cold (slow), trapped (long interaction time) samples. Similar to cold atoms, cold molecules could be interrogated at a level of detail which is likely to provide new insights into the structure and interactions of the much more complex molecule. We list below a few of the important areas of potential applications.

It should be possible to trap YbF, a proposed candidate for use in the search for an elementary electric dipole moment (a test of time reversal symmetry).[9,10] Using trapped YbF as a source of cold molecules could dramatically increase the sensitivity of such experiments.[11] Other, similar molecules are also the subject of investigation for use in experiments to observe both parity and time reversal violation.[12]

† Also at the Department of Chemistry and Chemical Biology, Harvard University, Cambridge, MA 02138, USA.

An exciting possible application of trapped molecules is in the area of lithography. Ultra-cold sodium and chromium have been focussed onto a substrate using a light grid where the feature sizes are approximately 20 nm.[13,14] Work is now ongoing to use chemical procedures to make a deposited grid useful for microelectronics applications.[15] In an ideal scenario, one would be free to choose which atom or molecule to deposit.

There is extensive interest in the very low energy collisional relaxation of molecules.[16–18] The production of ultra-cold molecules would allow the study of collisions where the translational energy is smaller than the other relevant energy scales in the system. The technique offers the possibility of investigating low-temperature collisional relaxation processes from excited electronic and ro-vibrational states. In addition to providing fundamental information on the interaction of molecules, these studies would also determine the feasibility of

Table 1 Maximum magnetic dipole moments of ground-state atoms.[6,7] Here S, L and J are spin, orbital and total angular momentum quantum numbers, respectively, and g_J is the Lande factor

state $^{2S+1}L_J$	$g_J J$	element
$^2P_{1/2}$	0.333	B, Al, Ga, In, Tl
$^4F_{3/2}$	0.598	V, Ta
$^2S_{1/2}$	1.001	H, Li, Na, K, Cu, Rb, Ag, Cs, Au, Fr
$^2D_{3/2}$	1.199	Sc, Y, La, Lu, Ac
$^3F_2$	1.332	Ti, Zr, Hf
$^6D_{1/2}$	1.669	Cb, Nb
$^2P_{3/2}$	2.001	F, Cl, Br, I, At
$^5I_4$	2.413	Nd
$^3P_2$	3.002	O, S, Se, Te, Po
$^4S_{3/2}$	3.003	N, P, As, Sb, Bi
$^4I_{9/2}$	3.290	Pr
$^1G_4$	3.782	Ce
$^6H_{5/2}$	3.782	Pm
$^2F_{7/2}$	3.994	Tm
$^3D_3$	4.002	Pt
$^3F_4$	5.002	Ni
$^6S_{5/2}$	5.006	Mn, Re, Tc
$^9D_2$	5.303	Gd
$^4F_{9/2}$	6.003	Co, Rh, Ir
$^5D_4$	6.005	Fe, Os
$^7S_3$	6.007	Mo, Cr
$^3H_6$	6.983	Er
$^5F_5$	7.005	Ru
$^8S_{7/2}$	7.007	Eu
$^4I_{15/2}$	8.964	Ho
$^5I_8$	9.933	Dy
$^6H_{15/2}$	9.938	Tb

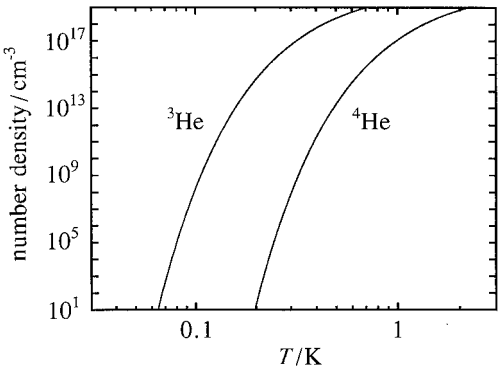

Fig. 1 Low-temperature number density curves of ^{3}He and ^{4}He. Note that the number density of *ca.* 10^{16} cm^{-3} required for buffer-gas loading (see text) is attained at 240 mK in ^{3}He and 800 mK in ^{4}He.

loading atoms and molecules in very long-lived metastable states.

High resolution spectroscopy of cold molecules would be relevant to the study of molecular structure and the precision testing of molecular theory. For example, trapped molecules could be used to study highly forbidden transitions. It is also conceivable that such research would impact on the area of coherent control: the long interaction time available could make it easier to tailor the internal wavefunctions of the molecules using external fields.

The technique should also open up the unexplored territory of interactions of ultra-cold gases of molecules whose axes could, in some cases, be spatially oriented.[8,19–21] This would enhance the dynamical resolution of many spectroscopic and collisional experiments since it eliminates averaging over random spatial orientations. Such polarization is possible when the electronic angular momentum is coupled to the molecular axis, as in Hund's cases (a) and (c). The molecular states that can be trapped coincide with the oriented precessing states of molecules.[8]

Although high-power CW lasers are not available in the UV range, frequency doubled sources operating at very low power levels suffice for the detection of both trapped atoms and molecules. The detection is straightforward. The creation of low-temperature samples of molecules may allow loading of the far-off-resonance optical trap.[22,23] The use of the FORT provides the additional possibility of doing spectroscopy with no magnetic field present. It may be possible to use buffer-gas loading to fill a FORT directly with molecules.[24]

The technique could also play a role in the study of collective quantum effects. It is known that the efficacy of evaporative cooling depends critically on the ratio of the dipolar relaxation cross-section to the elastic cross-section. For a review of the literature on evaporative cooling see ref. 25. There is an extreme sensitivity of this ratio to subtle details of the interaction potential. The exact effect of these cross-sections on the behavior of the Bose condensate is an open question. Also, the elastic cross-sections determine the stability of the condensate.[26–28] Using a variety of different atoms (or molecules) to form a condensate could help in understanding this new form of matter.

3 Buffer-gas loading

The technique of buffer-gas loading relies on thermalization of the species-to-be-trapped *via* collisions with a cold buffer gas. The buffer gas serves to dissipate the translational energy of the atoms or molecules, allowing them to sink into the conservative magnetic trapping field. Since this dissipation scheme does not depend on any particular energy level pattern, many atoms and molecules are amenable to it. As in the case of evaporative cooling of a trapped ensemble, buffer-gas loading relies on elastic collisions and, therefore, is of similar generality.

At temperatures of *ca.* 1 K, all stable substances except for He have negligible vapor pressure so the question arises as to how to bring the species-to-be-trapped into the gas phase. We found that laser ablation represents a particularly suitable means, although it is not the only one. Metal atoms can be efficiently vaporized by ablating a piece of solid metal; it is also possible to 'prepare' molecules, of varying complexity, by ablation of a suitable precursor.[29] In what follows we assume that the atoms or molecules are introduced into the gas phase by laser ablation.

The thermalization process can be modelled by assuming elastic collisions between two mass points m (buffer-gas atom) and M (species-to-be-trapped). From energy and momentum conservation in a hard-sphere model and by applying thermal averaging we find that the difference, ΔT, in temperature of the atom or molecule before and after a collision with the buffer-gas atom is given by $\Delta T = (T' - T)/\kappa$, with T the temperature of the buffer gas, T' the initial temperature of the atom or molecule, and $\kappa \equiv (M + m)^2/(2Mm)$; κ is equal to 26 for Eu atoms in ^{3}He buffer gas. The equation for the temperature change can be generalized and recast in differential form:

$$dT_N/dN = -(T_N - T)/\kappa \quad (1)$$

where T_N is the temperature of the atom or molecule after N collisions with the buffer-gas atom. Eqn. (1) has a solution

$$T_N = (T' - T)\exp(-N/\kappa) + T \quad (2)$$

Hence the number of collisions required for the atoms to fall within +30% of the ^{3}He buffer at $T = 0.25$ K is 250 for Eu at $T' = 1000$ K. In order to ensure that the atoms thermalize before impinging on the wall of the cell surrounding the trap (where, presumably, they would stick and be lost), it is necessary that the density of the buffer gas be large enough to allow for thermalization on a path smaller than the size of the cell (*i.e.* on the order of 1 cm). Assuming an elastic collision cross-section of about 10^{-14} cm^2 between the Eu atoms and ^{3}He, the minimum density required is on the order of 10^{16} cm^{-3}. This requirement together with attainable trap depths determines the necessary temperature of the buffer gas. Fig. 1 shows the dependence of number density on temperature for ^{3}He and ^{4}He at about 1 K.[30,31] One can see that ^{3}He (which has the highest number density of any stable substance at low temperatures) is suitable for thermalization at temperatures as low as 240 mK.

4 Buffer-gas loading and magnetic trapping of Eu atoms

Survey

The apparatus and the basic experimental procedure used in the trapping of Eu were described in ref. 4. Here we briefly summarize the main points. A schematic of the apparatus is shown in Fig. 2. Atomic europium is produced by laser ablation in a cryogenic cell filled with either ^{3}He or ^{4}He gas and thermalized in collisions with the He buffer. The cell is placed in an anti-Helmholtz field (magnetic field depth $H_{max} = 3$ T) which traps atoms in low-field seeking states whose kinetic energies are below the trap depth. The top of the cell is thermally anchored to the mixing chamber of a dilution refrigerator. The cell is filled with enough He to yield equilibrium density at temperatures of around 1 K. The cell is made of copper and is outfitted with a mirror on the inner top surface and a fused silica window on the bottom.

The atoms are detected *via* absorption spectroscopy in the a $^8S_{7/2} \rightarrow$ y $^8P_{7/2}$ band at 462.7 nm. The laser probe beam is produced by doubling the output of an actively stabilized

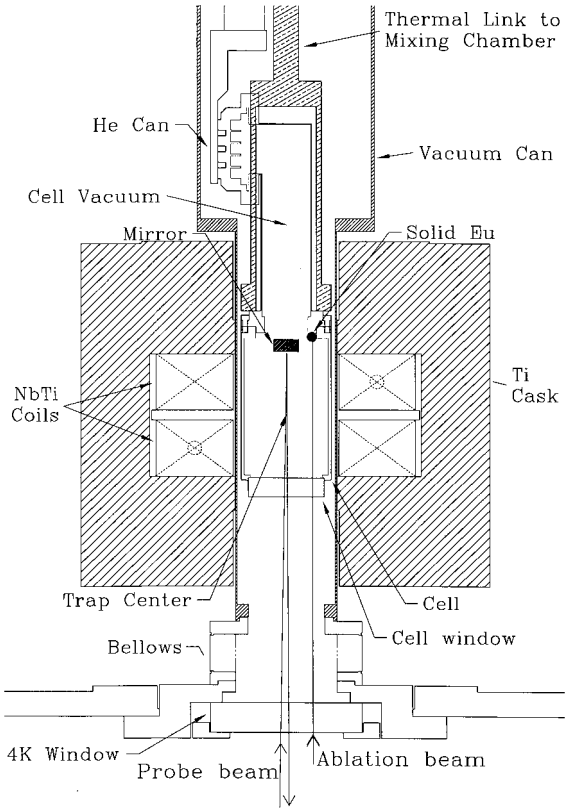

Fig. 2 Schematic diagram of magnetic trapping and optical detection apparatus. The superconducting magnet is immersed in liquid helium. Optical access to room temperature is provided by a set of borosilicate and fused silica windows at the cell temperature, 4 K, 77 K and 300 K. Only the 4 K window is shown. The 77 K and 300 K windows lie directly below the 4 K window. The YAG beam and the probe beam enter through the same set of windows.

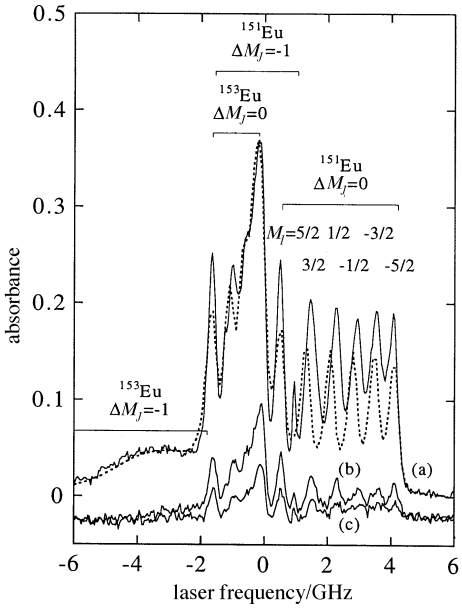

Fig. 3 Sample absorption spectra of the trapped ensemble of Eu at 0.6 T in the a $^8S_{7/2}$–y $^8P_{7/2}$ band at 462.7 nm measured (a) 20 s, (b) 40 s, and (c) 60 s after the ablation pulse. For clarity, the (b) and (c) spectra are shifted on the absorption scale by −0.025. The simulated spectrum, shown by the dotted line, provides the indicated assignment of the lines: all features are due to the $M_J = 7/2$ state of Eu($^8S_{7/2}$). For each isotope, there are two sub-bands of magnetic hyperfine transitions, with $\Delta M_J = 0$ and −1. Note that for the $\Delta M_J = 0$ transitions in ^{151}Eu, all six M_I nuclear spin states are clearly resolved.

Ti:sapphire laser (Coherent 899-21) in a $KNbO_3$ crystal. The typical power used to probe the atoms was 0.1 μW. A double pulsed YAG laser beam (Continuum I-10, 532 nm, 5 ns pulse width, 10 mJ typical pulse energy) was used to ablate Eu metal (99.9% pure, with the ^{151}Eu and ^{153}Eu isotopes in their natural abundances of 48% and 52%, respectively). The incoming probe beam (of a variable diameter) enters at an angle with respect to the cell axis and passes the cell center with an offset before impinging on the mirror at the top. The beam then reflects, passes the cell center with about the same offset, exits the cell, and is detected by a photomultiplier tube.

Loading of the trap, with the magnet on, begins by raising the cell temperature in order to increase the He number density; a resistor mounted on the top of the cell is used as a heater. A single YAG pulse is fired to ablate Eu and the heater is turned off. The temperature of the cell rises for *ca.* 1 s due to heating by the YAG pulse but then quickly decreases. We either (a) scan the laser over the whole absorption band at given delay times with respect to the ablation pulse, or (b) measure the absorption time profiles at given wavelengths. The former is possible because of the retention of the atoms due to trapping. Since the laser can be scanned at a rate of 130 GHz s^{-1}, the absorption spectrum can be measured more than ten times during 1 s, yielding good signal to background ratios.

Spectroscopy of trapped Eu

Fig. 3 shows sample spectra of the trapped Eu atoms at $H_{max} = 0.6$ T loaded using ^{3}He buffer at 0.25 K, taken 20, 40 and 60 s after the ablation pulse. The dotted line shows the corresponding simulation. The simulated trap spectrum was composed from the individual spectra calculated for a given value of the H-field and from the distribution function $N(H)$ of the number of atoms subject to a given H-field. The latter was determined for a given eigenstate and temperature from the calculated spatial distribution of the H-field and the factors accounting for the probe beam geometry. Thus, apart from the field distribution and the geometrical factors, the spectrum is determined entirely by temperature and the identity of the states trapped.

Fig. 4 shows a correlation diagram between the field-free states of ground-state Eu atoms and the corresponding high-field limit. There are 48 magnetic states for each Eu($^8S_{7/2}$) isotope due to the coupling of electronic angular momentum J with nuclear spin ($I = 5/2$ for either isotope).

As corroborated in our measurements at $H = 0$, the initial field-free populations of the Eu atoms are determined essentially by the degeneracy factors, $P(F) \rightarrow (2F + 1)$, *i.e.* all low-field states $|F, M\rangle$ have the same weight. In the high-field limit, the initial populations of the $|M_J, M_I\rangle$ states are determined by adiabatic transfer of the $|F, M\rangle$ states. The intensities, I, of the transitions between states in absorption spectra are then given by $I = PS$ where S is the line strength. At $H_{max} = 0.6$ T, more than 90% of the detected trapped atoms are subject to $H > 0.05$ T where the strong-field limit is reached (the Paschen-Back hyperfine uncoupling). As a result, the trap spectrum of Eu can be simulated analytically, with eigenenergies

$$E(M_J, M_I) = M_J g_J \mu_B H + M_I g_I \mu_B H + aM_J M_I + \frac{9b}{4I(2I-1)J(2J-1)} \times [M_J^2 - \tfrac{1}{3}J(J+1)][M_I^2 - \tfrac{1}{3}I(I+1)] \quad (3)$$

where J and I are the electronic and nuclear angular momentum quantum numbers ($J = 7/2$ for both electronic states), M_J and M_I their projections on the space fixed axis, g_J and g_I the corresponding g-factors, a and b the hyperfine magnetic dipole and electric quadrupole coupling constants,[32] and μ_B the Bohr magneton. The corresponding line strength factors $S_q(M'_J, M'_I;$

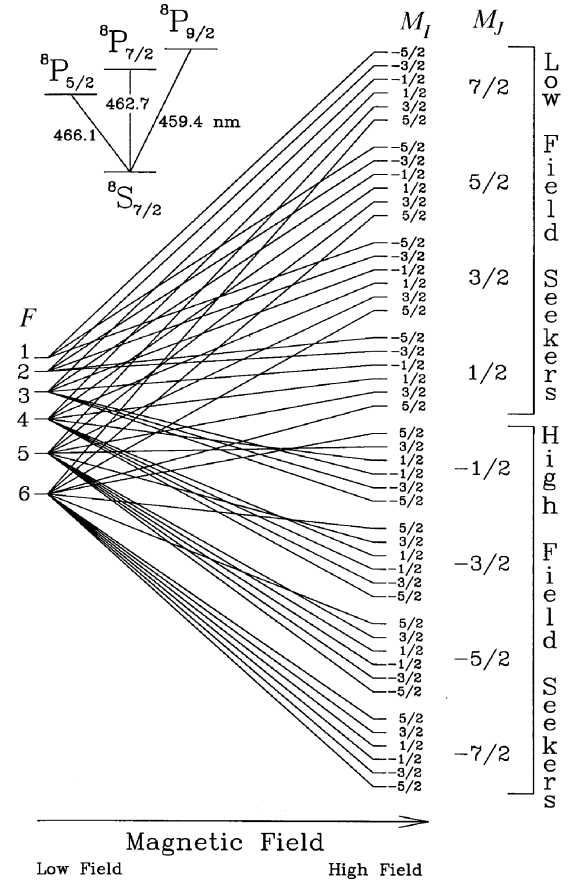

Fig. 4 Correlation diagram between the low- and high-field states for either of the stable isotopes of Eu(a $^8S_{7/2}$). Also shown is the transition to the y $^8P_{7/2}$ used to probe the atoms.

M_J, M_I) of electric dipole transitions between states $|M_J', M_I'\rangle \leftarrow |M_J, M_I\rangle$ are

$$S_q \propto \delta(M_I', M_I)\langle J, M_J, J', M_J'; 1, q\rangle^2 \quad (4)$$

with $q = 0$ for parallel and $q = \pm 1$ for perpendicular transitions.

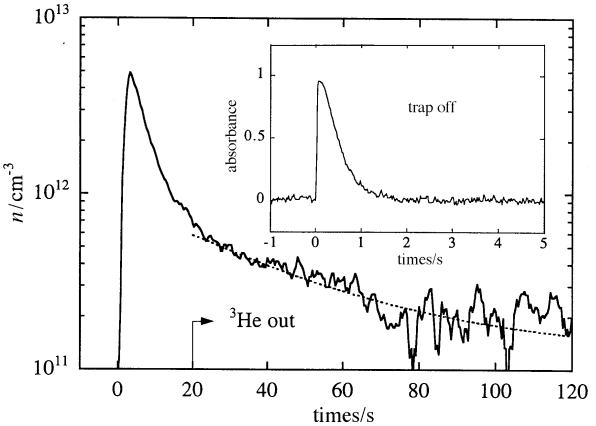

Fig. 5 Averaged absorption time profiles (full line) for ^{3}He loading at 250 mK measured at a fixed frequency of the laser (close to the band origin). A total of eight profiles were averaged. Note that about 20 s after the ablation pulse (time zero) the density of the buffer gas drops to about 5×10^{11} cm^{-3} (designated as ^{3}He out). The data are fitted with a combined one-body and two-body loss rate function (dashed line). About 1×10^{12} atoms are initially loaded into the trap using ^{3}He as a buffer gas. It was experimentally determined that optical pumping was negligible at the probe power levels used. The inset on the right shows an absorption time profile measured under the same conditions but with the trap off.

From the simulations it follows that essentially only the $M_J = 7/2$ state is trapped (in accordance with our model of loading). The corresponding simulated spectrum together with the assignment of the lines according to the isotope and hyperfine substate is also shown in Fig. 3. With this assignment, the temperature of the atoms in ^{3}He could be determined to be 250 ± 30 mK.

Absorption cross-section

In the low-optical density regime, the number of atoms in the trap can be obtained directly from the power absorbed $A \equiv 1 - P_f/P_i$, where P_i and P_f are the initial and final power, respectively. For an absorption cross-section $\sigma(\nu)$, density of the medium $n(x, y, z)$, and a uniform laser beam with cross-section Φ

$$A(\nu) = 1 - \frac{1}{\Phi}\int_x\int_y \mathrm{d}x\,\mathrm{d}y\,\exp\left(-\int_z \sigma(\nu(x, y, z))n(x, y, z)\,\mathrm{d}z\right) \quad (5)$$

For atoms inside a magnetic trap,

$$n(x, y, z) = n_0 \exp\left[-\frac{E(H(x, y, z))}{kT}\right] \quad (6)$$

where n_0 is the number density at the trap center, $E(H(x, y, z))$ the eigenenergy ($E > 0$ for trappable states), and z the cell axis. Hence the number of atoms and their central density can be extracted from the absorption profile if the magnetic field distribution, temperature, beam geometry and the absorption cross-section are known. Note that the absorption cross-sections for untrapped and trapped atoms are different. This is due to an inhomogeneous broadening by the magnetic trapping fields.

Fig. 5 shows the absorption time profiles at fixed laser frequency (corresponding to maximum absorption) for ^{3}He loading with the magnet on and off (see the inset). The absolute atom number was determined from the simulation of the spectra and the published line strength factors.[33,34] An initial density of 5×10^{12} cm^{-3} with an initial atom number of 1×10^{12} was achieved. The data were fitted assuming a combined one-body and two-body loss. From this we determined a two-body (Eu–Eu) collisional loss rate constant $(2.5 \pm 1.5) \times 10^{-13}$ cm^3 s^{-1} at 170 mK. Unlike the ^{4}He case, here the sample is in thermal contact with the cell wall. Fits performed assuming a three-body process (Eu–Eu–Eu) yielded similar quality results to the two-body fits. Thus three-body loss cannot be ruled out although it seems unlikely given the Eu densities present in the trap.

In recent work we used the buffer-gas technique to load atomic ^{52}Cr into a magnetic trap. As with Eu, the initial densities were above 10^{12} cm^{-3}. The chromium experiment was carried out with a single isotope, ^{52}Cr, that has zero nuclear spin and thus, unlike Eu, no hyperfine structure. This is the subject of a forthcoming paper.[5]

5 Magnetic trapping of molecules

It should be possible to trap and evaporatively cool molecular oxygen. We consider $O_2(X\,^3\Sigma_g^-)$ to be a prototype 2 μ_B species. Fluorescence spectroscopy in the A-band could be used to measure the temperature and density of the trapped sample as it is evaporatively cooled. From this, the low-energy elastic and inelastic collision cross-sections can be deduced. We consider $NO(X\,^2\Pi_{3/2})$ to be a prototype 1 μ_B system. It is possible to supplement the magnetic trapping field with a congruent electric field, enabling the separation of molecular states with negative and positive projections of the electronic angular momentum on the figure axis.[8]

Depending on the electronic structure of a given molecular state, the electronic angular momentum (and hence the electronic magnetic dipole moment) tends to couple either to the molecular axis, as in Hund's cases (a) and (c), or to the rotational angular momentum, as in Hund's case (b). Magnetic properties of molecules with these two types of coupling differ considerably, although both give rise to states with non-zero space-fixed magnetic dipole moments, and are suitable for trapping. For instance, $O_2(X\,^3\Sigma_g^-)$ comes close to Hund's case (b), while $NO(X\,^2\Pi_{3/2})$ approaches Hund's case (a). Moreover, NO has also an electric dipole moment (inherently coupled to the molecular axis) whose interaction with a congruent electric field can also be exploited; therefore, for Hund's case (a) we present a generalized treatment for parallel electric and magnetic fields.

Eigenproperties

Hund's case (a) molecules in congruent electric and magnetic fields. The eigenfunctions of a polar paramagnetic rigid linear molecule subject to parallel uniform electric, ϵ, and magnetic, H, fields are hybrids of the field-free symmetric top wavefunctions $|J, \Omega, M\rangle$

$$|\tilde{J}, \Omega, M; \omega_\pm\rangle = \sum_{J=\max(|\Omega|, |M|)}^{\infty} a_{J\Omega M}(\omega_\pm)|J, \Omega, M\rangle \qquad (7)$$

here Ω and M are projections of the total angular momentum, $\boldsymbol{J}$, (electronic and rotational, but excluding nuclear spin) on the figure and space-fixed axes, respectively. The Fourier coefficients $a_{J,\Omega,M}$ depend solely on the interaction parameter $\omega_\pm \equiv \omega_{el} \pm \omega_m$, where $\omega_{el} \equiv \mu_{el}\epsilon/B$ and $\omega_m \equiv \mu_m H/B$ are dimensionless parameters which measure the potential energy of the electric, μ_{el}, or magnetic, μ_m, dipole moment component along the molecular z-axis in units of the rotational constant, B. The range of J, the total angular momentum quantum number, involved in a hybrid wavefunction $|\tilde{J}, \Omega, M; \omega_\pm\rangle$ increases with the $\omega_\pm$ parameter. The eigenstates are labeled by $\tilde{J}, \Omega, M$ where $\tilde{J}$ denotes the nominal value of J that pertains to the field-free rotational state which adiabatically correlates with the high-field state, $|\tilde{J}, \Omega, M; \omega_\pm \to 0\rangle \to |J, \Omega, M\rangle$. In the field-free limit the eigenenergies are $E_{J\Omega}/B = J(J+1) - \Omega^2$. In the high-field limit, the hybrid states become harmonic, corresponding to those of an angular oscillator with energies $E_v/B = -\omega_\pm + v(2\omega_\pm)^{1/2} - \Omega^2$, where $v \equiv 2\tilde{J} - |M + \Omega|$.

The body-fixed electronic magnetic dipole moment endowed by the electronic angular momentum is $\mu_m = (g_L\Lambda + g_S\Sigma)\mu_B$ where $\Lambda = 0, \pm1, \pm2, \ldots$ and $\Sigma = 0, \pm1, \pm2, \ldots$ or $\pm1/2, \pm3/2, \ldots$ are projections of the orbital and spin electronic angular momenta $\boldsymbol{L}$ and $\boldsymbol{S}$ on the z-axis, g_L and g_S are the respective gyromagnetic ratios ($g_L = 1$, $g_S \approx 2.00229$), and μ_B is the Bohr magneton. Since states differing in the sign of $\Omega = \Lambda + \Sigma$, Λ and Σ are equally populated, half of the molecules have μ_m and ω_m positive and half have μ_m and ω_m negative. The body-fixed electric dipole moment μ_{el} (and thus ω_{el}) is along the molecular z-axis and its direction is fixed in a given electronic state. Consequently, in parallel electric and magnetic fields, half of the molecules have $\omega = \omega_{el} + \omega_m \equiv \omega_+$ and half have $\omega = \omega_{el} - \omega_m \equiv \omega_-$.

The expectation value of the cosine of the angle θ between the field direction and the figure axis is given by

$$\langle\cos\theta\rangle = \sum_{J,J'=0}^{\infty} a_{J\Omega M}(\omega_\pm)a_{J'\Omega M}(\omega_\pm)(2J+1)^{1/2}(2J'+1)^{1/2} \times \begin{pmatrix} J & 1 & J' \\ -M & 0 & M \end{pmatrix}\begin{pmatrix} J & 1 & J' \\ -\Omega & 0 & \Omega \end{pmatrix} \qquad (8)$$

for precessing states (*i.e.* states with non-zero J, Ω, M) at $\omega_\pm \to 0$ this gives $\langle\cos\theta\rangle = \Omega M/[J(J+1)]$. As a result, the corresponding low-field energy (*i.e.* due to first-order Stark and/or Zeeman effect),

$$E_{J\Omega M}/B = -\langle\cos\theta\rangle\omega_\pm \qquad (9)$$

is negative for $\omega_\pm > 0$ and $\Omega M > 0$ (*i.e.* for $\omega_\pm M\Omega > 0$) and positive for $\omega_\pm > 0$ and $\Omega M < 0$ (*i.e.* for $\omega_\pm M\Omega < 0$). Since the sign of $\omega_\pm M\Omega$ remains the same at all field strengths, the multiplets with $\omega_\pm M\Omega < 0$ are always higher in energy than those with $\omega_\pm M\Omega > 0$.

In a given electronic state and at given non-zero M, Ω, ω_{el}, and ω_m, there are 2^2 sign combinations since the signs of ω_m and Ω are the same and the sign of ω_{el} is fixed. These give rise to a quadruplet of non-degenerate states, consisting of two doublets, one with $\omega_+ = \omega_{el} + \omega_m$ and the other with $\omega_- = \omega_{el} - \omega_m$. This situation is referred to as the $\omega_\pm M\Omega$ rule. An important special case arises within the realm of the $\omega_\pm M\Omega$ rule: for $\omega_{el} = \omega_m \equiv \omega$ we obtain $\omega_+ = 2\omega$ and $\omega_- = 0$. As a result, the quadruplet of states with given non-zero M, Ω, ω_{el}, and ω_m degenerates into two hybrid states and two free-rotor states.

The requisite field-dependence of eigenenergy for low-field seeking states occurs for $\langle\cos\theta\rangle < 0$. In the purely electric case ($\omega_{el} > 0$, $\omega_m = 0$), the states $|\tilde{J}, \Omega, M; \omega_{el}\rangle$ and $|\tilde{J}, -\Omega, -M; \omega_{el}\rangle$ have the same $\langle\cos\theta\rangle$ as do the states $|\tilde{J}, -\Omega, M; \omega_{el}\rangle$ and $|\tilde{J}, \Omega, -M; \omega_{el}\rangle$, cf. the $\omega_\pm M\Omega$ rule. Consequently, the deflection in an inhomogeneous electric field, proportional to $\omega_{el}\langle\cos\theta\rangle$, is the same for $+\Omega$ and $-\Omega$. In the purely magnetic case ($\omega_{el} = 0$, $\omega_m \neq 0$), the term $\omega_m\langle\cos\theta\rangle$ is positive definite, leading again to the same deflection for the $+\Omega$ and $-\Omega$ states. Likewise, optical transitions cannot favor any of the $+\Omega$ or $-\Omega$ states as the $|\tilde{J}, \Omega, M; \omega_{el}\rangle$, $|\tilde{J}, -\Omega, -M; \omega_{el}\rangle$ or $|\tilde{J}, \Omega, M; \omega_m\rangle$, $|\tilde{J}, -\Omega, M; -\omega_m\rangle$ and $|\tilde{J}, -\Omega, M; \omega_{el}\rangle$, $|\tilde{J}, \Omega, -M; \omega_{el}\rangle$ or $|\tilde{J}, \Omega, -M; \omega_m\rangle$, $|\tilde{J}, -\Omega, -M; -\omega_m\rangle$ pairs of states are degenerate. Consequently, pairs of $\pm\Omega$ states behave like racemic mixtures of isomers, not inconvertible by radiation or separable by an external electric or magnetic field.

However, the combination of parallel electric and magnetic inhomogeneous fields does offer a means to separate the $+\Omega$ and $-\Omega$ states. This separation scheme is based on the $\omega_\pm M\Omega$ rule, yielding deflections proportional to $\omega_\pm\langle\cos\theta\rangle$. For $|\omega_{el}| \leqslant |\omega_m|$, the expectation values of the orientation cosine for the $|\tilde{J}, \Omega, M; \omega_+\rangle$ and $|\tilde{J}, -\Omega, -M; \omega_-\rangle$ states are positive so that these states would be defocused (and thus discarded) in the combined fields. On the other hand, the $|\tilde{J}, -\Omega, M; \omega_-\rangle$ and $|\tilde{J}, \Omega, -M; \omega_+\rangle$ states are focusable, with $\langle\cos\theta\rangle < 0$. As long as $\omega_+ \neq \omega_-$, their respective orientation cosines are different, leading to different interaction energies that enable separation. In the special case when $|\omega_{el}| = |\omega_m|$, the energies of the $|\tilde{J}, -\Omega, M; \omega_-\rangle$ and $|\tilde{J}, -\Omega, -M; \omega_-\rangle$ states would be zero, since $\omega_- = 0$. The $|\tilde{J}, \Omega, M; \omega_+\rangle$ state would be discarded because of its positive $\langle\cos\theta\rangle$. Then only the $|\tilde{J}, \Omega, -M; \omega_+\rangle$ state would be trapped at field strengths ω_+ preserving its negative $\langle\cos\theta\rangle$.

Since the quadruplet of states within the $\omega_\pm M\Omega$ rule is non-degenerate, preferential populations of either the $+\Omega$ or $-\Omega$ states could also be created by optical transitions.

Hund's case (b) molecules in a magnetic field. In Hund's case (b), the electronic angular momentum, $\boldsymbol{L} + \boldsymbol{S}$, couples to the rotational angular momentum, $\boldsymbol{N}$, of the linear molecule. Here we consider the case when $\boldsymbol{L} = 0$ so that the electronic angular momentum is solely due to the electronic spin, $\boldsymbol{S}$. The spin gives rise to a body-fixed spin magnetic dipole moment $\mu_S = -g_S[S(S+1)]^{1/2}\mu_B$, with S the spin angular momentum quantum number. The coupling of $\boldsymbol{S}$ and $\boldsymbol{N}$ results in total angular momentum $\boldsymbol{J}$ with projection M on the space-fixed axis, Z, defined by the direction of an external magnetic field H. The expectation value of the space-fixed magnetic dipole

moment is then given by

$$\langle \mu_Z \rangle = \mu_S \langle \cos \chi \rangle \langle \cos \alpha \rangle \tag{10}$$

where χ is the angle between $\boldsymbol{S}$ and $\boldsymbol{J}$ and α is the tilt angle of $\boldsymbol{J}$ with respect to Z. Since $M = -J, -J+1, \ldots, J-1, J$ is a good quantum number for the molecular magnetic dipole,

$$\langle \cos \alpha \rangle = \frac{M}{[J(J+1)]^{1/2}} \tag{11}$$

the expectation value of $\langle \cos \chi \rangle$ is given by

$$\langle \cos \chi \rangle = \frac{J(J+1) + S(S+1) - N(N+1)}{2[J(J+1)S(S+1)]^{1/2}} \tag{12}$$

as follows from the law of cosines.

Although the molecular eigenstates cannot be hybridized by the magnetic field (unless there is some coupling of $\boldsymbol{S}$ to the internuclear axis, which is actually the case for ground-state O_2), they can be deflected and thus trapped by the interaction of the space-fixed dipole moment with an inhomogeneous magnetic field H.

The magnetic eigenenergies in the $|J, N, S, M; \omega_S\rangle$ states are given by

$$E_{JNSM}(\omega_S) = -\langle \mu_Z \rangle_{JNSM} H \tag{13}$$

where $\omega_S \equiv \mu_S H/B$ measures the maximum potential energy of the magnetic dipole in terms of the rotational constant of the molecule. Thus the field-dependence of the magnetic energy required for trapping occurs for $\langle \mu_Z \rangle < 0$.

For a $^2\Sigma$ molecule (*i.e.* $S = 1/2$), J can take non-negative values $N + 1/2$ [the so called $F_{N+1/2}(J)$ term] or $N - 1/2$ ($F_{N-1/2}$ term), with $N = 0, 1, 2, \ldots$. So for instance the magnetic energy shift of the $F_{N-1/2}(1/2)$ term for $N = 1$ is given by $E_{1/2,\,1,\,1/2,\,M} = Mg_S\mu_B H/3$; for a $^3\Sigma$ molecule (*i.e.* $S = 1$), J can take non-negative values $N + 1$ [the so called $F_{N+1}(J)$ term], N [$F_N(J)$ term], or $N - 1$ [$F_{N-1}(J)$ term], with $N = 0, 1, 2, \ldots$. The magnetic energy shift of the $F_{N+1}(1)$ term for $N = 0$ is then $E_{101M} = Mg_S\mu_B H$.

Magnetic trapping of O_2

The O_2 molecule offers an easily accessible optical transition in the near-IR part of the spectrum. It should be possible to determine the number of the molecules and their temperature by measuring the spatial distribution of the trapped sample or by exciting the whole sample and measuring a frequency spectrum. The total number of molecules could be roughly determined from the signal level and more accurately from the signal levels in combination with the measured temperature of the sample.

Buffer-gas loading. Fig. 6 shows energies of states in the two lowest rotational manifolds ($N = 1, 0$).[35,36] Which states are populated depends on the identity properties of the oxygen nuclei. For $^{16}O_2$ and $^{18}O_2$ and $^{17}O_2$ with even total nuclear spin, only the odd N manifolds can be occupied. For $^{17}O_2$ with odd total nuclear spin, only the even N manifolds can be occupied. For mixed isotopes (for example $^{16}O^{18}O$) there is no restriction. In principle we could load in any isotope combination because there exist trappable states with $\langle \mu \rangle = 2\mu_B$ magnetic moment in either manifold. It is possible, however, that during the loading process the total angular momentum quantum number (J) could relax to be in equilibrium with the translational degrees of freedom which are at 240 mK. The rate of this relaxation based upon higher temperature measurements may be large enough for this to occur. For the even isotopes, the ($N = 1$, $J = 1$, $M = 1$) state could relax to the ($N = 1$, $J = 0$) state which is not trappable. For the mixed isotopes and $^{17}O_2$, the $N = 0$ manifold is 1.78 cm^{-1} lower

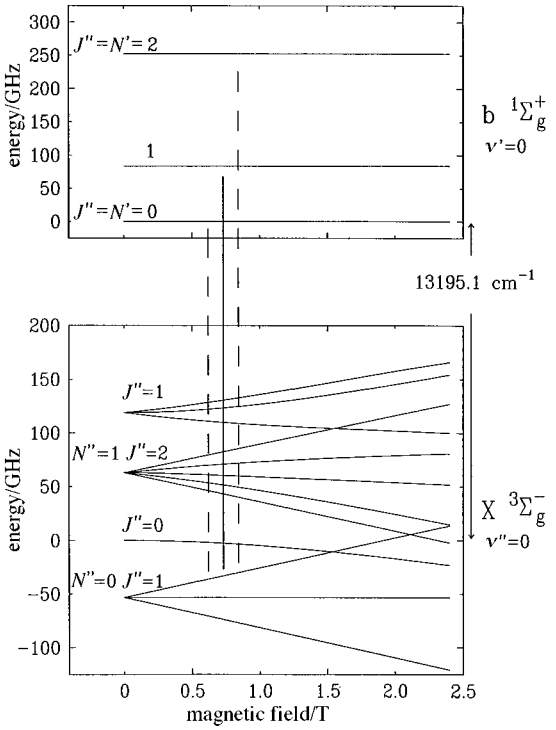

Fig. 6 Eigenenergies and their field dependence for the lowest states of O_2 within the electronic ground state $X\,^3\Sigma_g^-$ ($v'' = 0$) and the $b\,^1\Sigma_g^+$ ($v' = 0$) excited state. See text.

than the ($N = 1$, $J = 0$) state.[37] There is, however, a series of level crossings that begin to occur at 1.5 T. It is possible that the desirable ($N = 0$, $J = 1$, $M = 1$) state could make transitions to untrapped states as the molecule moved through those regions of the magnetic field. The case of $^{17}O_2$ with odd total nuclear spin does not allow this possibility. The $N = 1$ state cannot be populated so that only the $N = 0$ state needs to be considered. With zero rotation, only the spin of the electrons is important and transitions between the states in that manifold proceed *via* dipolar (or higher order spin) relaxation collisions. $^{17}O_2$ will have a hyperfine structure (the spin of the nucleus is 5/2)[38] and thus spin-exchange collisions are possible.[2] This is similar to the case of atomic hydrogen trapping and it might be expected that these collisions will quickly leave the gas of molecules in a state with pure spin where both the nuclear and electronic spins are oriented. Studies of rotational relaxation collisions, spin-exchange collisions and non-adiabatic transitions are important and could be investigated.

Laser detection of trapped molecular oxygen. The detection technique of choice is fluorescence spectroscopy in the $b\,^1\Sigma_g^+(v' = 0) \leftarrow X\,^3\Sigma_g^-(v'' = 0)$ band (the A-band). The Einstein A coefficient for this band has been measured to be 0.087 s^{-1}.[39] The transition rate per molecule can then be determined to be

$$W[s^{-1}] = 2 \times 10^{12} \frac{P[\text{watts}]}{\Phi[cm^2]\Delta\nu[GHz]} A[s^{-1}]\nu^{-3}[cm^{-1}]$$

$$= 0.077 \frac{P}{\Phi\Delta\nu} \tag{14}$$

where P is the power of the laser beam exciting the transition, $\Delta\nu$ the effective linewidth of the transition, and Φ the cross-sectional area of the laser beam. Here it is assumed the linewidth of the laser is matched to the linewidth of the sample. The major broadening mechanism for the transition is magnetic field broadening. The state that the molecule is being excited to has zero electron spin whereas the ground state has

a magnetic moment of of 2 μ_B (28 GHz T^{-1}). The total broadening is given by $\Delta\nu = 20.8T$ GHz where T is the temperature of the molecules. The initial loading temperature would be 240 mK. Because most of the molecules are in a band $2kT$ wide in energy, magnetic broadening amounts to 5 GHz. Doppler broadening is negligible (<20 MHz at 240 mK). The $2kT$ energy band where most of the molecules reside is centered $2kT$ above the trap minimum, and so most of the molecules in the sample reside within about 1/8 of the radius of the cell. In order for the light to intersect all of these molecules, the beam diameter required is 0.6 cm. For a typical power of 2.5 W the per atom excitation rate is 0.13 s^{-1}. As will be shown later, the time for excitation may be short (limited by the time of flight of the excited molecule to the physical wall) so only a small fraction of the molecules are in the excited state and saturation does not occur. The lower temperatures attainable *via* evaporative cooling would narrow the linewidth of the sample and therefore improve the performance of the spectroscopic detection. Our conservative estimate for the number of trapped molecules immediately after loading is 3×10^{12}. Based on the 0.13 s^{-1} per molecule excitation rate the total excitation rate is 3×10^{11} s^{-1}. Through the proper use of light pipes and cooled photomultiplier tubes the total collection efficiency for the fluorescence could be made 1×10^{-3}. The length of time available to count may, however, be limited by the time of flight of the excited molecules; once excited, the molecules will travel outwards from the center of the cell and impinge on the walls. Although it may be that the surface collision induces a radiative transition, we assume here that they do not radiate during the adsorption process. The time the molecule spends traveling from near the center of the trap to the cell wall determines how much time it has to radiate. For an average speed, just after loading, of 1000 cm s^{-1} and for the cell radius of 2.5 cm, the resulting average time is 2.5 ms. Therefore, an experimental procedure could be to chop the laser beam at 200 Hz, 50% duty cycle, and look for fluorescence during the dark period. During the dark period the fluorescence rate would be 2×10^8 s^{-1} which would result in a count rate of 2×10^5 s^{-1}. Available cooled photomultiplier tubes have a background count rate of less than 10 s^{-1} so the expected signal to noise in 1 s of integration time would be 2×10^4. This high count rate should allow detailed spectra to be taken.

As the molecules are excited, they travel to the walls of the cell and are lost. Eventually all of the molecules are expelled from the trap. However, the signal to noise is high enough so that lower laser powers could be used to, for example, monitor atom number as the sample is evaporatively cooled. The total number of molecules could be determined by measuring the total fluorescence signal and relating that to the (all known) quantum efficiency of the PMT, laser power, excitation rate and geometrical factors. It should be possible to determine total atom number to better than a factor of 2. Narrowing the laser linewidth and scanning over the broad 5 GHz line would allow the determination of the energy distribution of the trapped sample. The number of molecules in a magnetic field shell dH centered around a magnetic field H is

$$N(H)\,\mathrm{d}H = 4\pi H^2\,\mathrm{d}H(\nabla H)^{-3} n_0 \exp\left(-\frac{\langle\mu\rangle H}{kT}\right) \qquad (15)$$

where ∇H is the magnetic field gradient produced by the trap. By determining the number of molecules at different magnetic field strengths and comparing to the above function, the temperature can be determined. It should be possible to determine the temperature with an accuracy of a few percent for the 240 mK sample. Also, it should be possible in certain cases to 'burn' a hole in the energy distribution and then measure the rate of filling. This would be a direct measure of the elastic cross-section.

Trapping and orientation of NO

Trapping and selection of $\pm\Omega$ states. Results from supersonic beam work indicate that both neat and seeded expansions of room tempearture NO leave about 1% or more of the molecules in the $X\,^2\Pi_{3/2}$ paramagnetic spin–orbit state.[40] This is the case even for strong expansions, where the number of collisions approaches 10^4. Therefore, we assume that NO($X\,^2\Pi_{3/2}$) could be subject to both buffer-gas loading of the magnetic trap and subsequent evaporative cooling. We expect that also discharge desorption of NO from the cold walls of the refrigerator would create significant amounts of NO in the $^2\Pi_{3/2}$ state.

The energy level diagram of the $X\,^2\Pi_{3/2}$ and the $A\,^2\Sigma^+$ manifolds (the latter of interest for detection of NO, see below) is shown in Fig. 7. The hyperfine structure, arising mainly due to quadrupole coupling of the nitrogen nucleus,[38] is not indicated for simplicity. The field dependence of the $|\tilde{J}, \Omega, M; \omega_m\rangle$ hybrids with $\tilde{J} = 3/2$ falls well within the first-order Zeeman effect at magnetic field strengths of up to 2 T. Although all four states with $\Omega M < 0$ are focussable, only those with $|M| = 3/2$ would be used for trapping; the space-fixed magnetic dipole moment of these states comes close to $\langle\mu\rangle \approx (3/5)\omega_m \approx (6/5)\mu_B$, yielding a trap depth of 3.3 K. Unlike the case of O_2, the electronic angular momentum of NO($X\,^2\Pi_{3/2}$) is coupled to the internuclear axis. Therefore, reorientation collisions may contribute to the relaxation of the focussable M-states within a given $\tilde{J}$-state manifold. The rate of this relaxation process can be roughly estimated as lower than rotational relaxation; our experiment will provide a more definitive answer. If the magnetic trapping of NO is successful, we plan to supplement the magnetic field with a congruent (or parallel) electric field and to attempt to separate the $|\tilde{J} = 3/2,\ \Omega = 3/2,\ M = -3/2;\ \omega_+\rangle$ and $|\tilde{J} = 3/2,\ \Omega = -3/2,\ M = 3/2;\ \omega_+\rangle$ by trapping just the latter state, cf. the $\Omega M\omega_\pm$ rule. Table 2 lists the expectation values and energies of the quadruplet of $|3/2, \pm 3/2, \pm 3/2;\ \omega_\pm\rangle$ states for easily attainable values of $\omega_{el} = \omega_m = 0.1$. It can be seen that the $\omega_- = 0$ states will not be affected by the fields at all, while the $|3/2,$

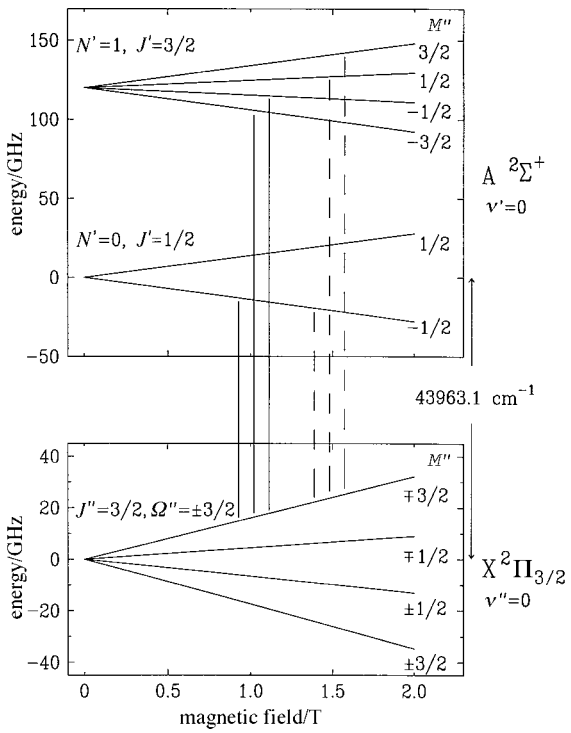

Fig. 7 Eigenenergies and their field dependence for the lowest states of NO within the electronic ground state $X\,^2\Pi_{3/2}$ ($v'' = 0$) and the $A\,^2\Sigma^+$ ($v' = 0$) excited state. See text.

Table 2 The separation of the $+\Omega$ states according to the $\omega \pm M\Omega$ rule for $\omega_{el} = \omega_m = 0.1$

state $\tilde{J}$, Ω, M; $\omega_\pm$	$\langle\cos\theta\rangle$	$E_{\tilde{J}\Omega M}/B$
$\|3/2, 3/2, 3/2; \omega_{el} + \omega_m\rangle$	+0.61	+0.122
$\|3/2, 3/2, -3/2; \omega_{el} + \omega_m\rangle$	−0.59	−0.118
$\|3/2, -3/2, -3/2; \omega_{el} - \omega_m\rangle$	+0.60	0
$\|3/2, -3/2, 3/2; \omega_{el} - \omega_m\rangle$	−0.60	0

$3/2, -3/2; \omega_+\rangle$ will be pushed towards the high-field edge of the trap and thus discarded. The only trapped state then would be the $|3/2, +3/2, +3/2; +\omega_+ = 0.2\rangle$ state.

Laser detection of $\pm\Omega$-selected NO. The NO molecules can be detected by laser induced fluorescence or absorption excited within the $A\,^2\Sigma^+_{1/2}$, $v' = 0 \leftarrow X\,^2\Pi_{3/2}$, $v'' = 0$ band at about 227 nm, cf. Fig. 7. The Einstein A-coefficient of the A state has been measured to be $A = 4.63 \times 10^6$ s^{-1} [41] so that the excitation rate per molecule at a laser spectral energy density $\rho = 1 \times 10^{-3}$ erg cm^{-2} is $W = 1 \times 10^5$ s^{-1}. With about 3×10^{12} molecules trapped this would give rise to fluorescence rates of about 1×10^{14} s^{-1} and thus to count rates on the order of 10^{11} s^{-1}.

The A-state comes close to Hund's case (b)[42] and the corresponding Zeeman states, $|J, N, S, M; \omega_S\rangle$, within the A, v' manifold will be designated as $|J', \Omega' = 0, M'; \omega_{S'}\rangle$. The transition probability for an electric dipole transition between a pair of states $|J', \Omega', M'; \omega'_S\rangle \leftarrow |J'', \Omega'', M''; \omega_\pm\rangle$ (analogous to the rotational line strength factor) is given by

$$S = \left| (2J'+1)^{1/2} \sum_{J'', Q, q} a_{J''\Omega''M''}(\omega_\pm)(2J''+1)^{1/2}(-1)^{M'} \times \begin{pmatrix} J'' & 1 & J' \\ -M'' & Q & M' \end{pmatrix} \begin{pmatrix} J'' & 1 & J' \\ -\Omega'' & q & \Omega' \end{pmatrix} \right|^2 \quad (16)$$

Here $Q = 0, \pm 1$ designates the spherical components in the space-fixed frame of the electric vector e_Q of the radiation and $q = 0, \pm 1$ those in the body-fixed frame of the transition dipole operator μ_q for the molecule; these are set equal to unity in this expression, $|e_Q| = |\mu_q| = 1$. For polarization parallel and photons propagating perpendicular to the direction of the fields, the only non-zero component of the photon angular momentum is along the parallel fields, *i.e.* for $Q = 0$. The $a_{J''\Omega''M''}$ coefficients introduced by the field-induced hybridization of J-states within the X, $v'' = 0$ state manifold give rise to non-zero transition probabilities between states that differ by more than unity in their nominal $\tilde{J}$-values. This enriches the spectra with transitions that would be forbidden in the absence of the hybridizing fields.

When both fields are present, *i.e.* $\omega_\pm \neq 0$, states with same $\tilde{J}$ and M but $\pm\Omega$ differ both in energy and wavefunction, according to the $\omega_\pm M\Omega$ rule. The corresponding transitions

$$\begin{aligned} &|J', 0, +M \pm \Delta M; \omega'_S\rangle \leftarrow |\tilde{J}'', +\Omega'', +M; \omega_+\rangle \\ &|J', 0, -M \pm \Delta M; \omega'_S\rangle \leftarrow |\tilde{J}'', -\Omega'', -M; \omega_-\rangle \\ &|J', 0, +M \pm \Delta M; \omega'_S\rangle \leftarrow |\tilde{J}'', -\Omega'', +M; \omega_-\rangle \\ &|J', 0, -M \pm \Delta M; \omega'_S\rangle \leftarrow |\tilde{J}'', +\Omega'', -M; \omega_+\rangle \end{aligned} \quad (17)$$

occur at different frequencies and with different probabilities. This is not the case when only the electric field is present: then the first two and the last two transitions are coinciding twins (degenerate). Thus the presence of the magnetic field makes the distinction possible between transitions involving states with positive or negative Ω. The trapping of only one of the $\pm\Omega$ states by the congruent (parallel) electric and magnetic fields would therefore be revealed by the disappearance of two of the above transitions; these are shown by the dashed lines in Fig. 7.

6 Conclusions

We have magnetically trapped atomic Eu using our buffer-gas loading technique. Because buffer-gas loading does not depend on the details of internal level structure, this demonstration has set the stage for loading of molecules into a magnetic trap using the same method.

Many ground-state molecules are paramagnetic and therefore amenable to magnetic trapping. Theory has been developed to describe magnetic trapping and spectroscopic detection of NO and O_2 molecules. These are 'prototype' species that fall, respectively, close to Hund's coupling cases (a) and (b). We conclude from our analysis that buffer-gas loading and magnetic trapping of these (and many other) molecules is feasible.

Just as atom trapping and cooling is now beginning to open up a wide range of possibilities for new experiments, we feel it is likely that the same will happen with molecular trapping and cooling.

Note added in proof

Recently, we carried out experiments on buffer-gas cooling of vanadium monoxide in a magnetic trapping field. We give a brief description of that work here and refer the reader to ref. 43.

VO($^4\Sigma^-$) molecules are produced by YAG pulses (20 mJ, 4 ns, 532 nm) impinging on a compacted and thermally processed sample of V_2O_5 placed in a cryogenic cell (<1 K) surrounded by a quadrupole magnetic trapping field; the cell is in thermal contact with a dilution refrigerator. Once produced, the VO diffuses through ^{3}He buffer gas and undergoes collisional relaxation, both translationally and internally. The VO molecules are detected within the $C\,^4\Sigma^- - X\,^4\Sigma^-$ band at 574 nm either by laser absorption or laser-induced fluorescence spectroscopy. The field free spectra were assigned in agreement with ref. 44 and used to determine both the translational temperature (from the Doppler widths) and the rotational temperature (from the intensity distribution of the rotational lines); the temperatures were found to be the same, equal to about 1 K. The spectra were measured at each frequency of the probe laser as a function of time (time profiles). From the spectra taken at different delay times we conclude that the thermalization with the buffer gas occurs within 10 ms of the ablation pulse. The time profiles also yield the rate at which the VO molecules disappear from the cell. The corresponding loss time constant is about 60 ms, a factor of five shorter than for Eu and Cr atoms. Since the atoms disappear predominantly by diffusion to the cell walls (where they stick), the dissimilarity of the decay times and other observations suggest that sticking to the walls is unlikely to be the limiting decay process for the VO molecules. Among the plausible loss mechanisms seem to be chemical reactions of the VO molecules with other molecules in the trap or sticking of the VO to the 'dust.' Both a variety of molecules and, presumably, some dust is produced during the ablation process. This is consistent with the observation that with the trapping field on, the decay rate of VO remains the same. The rapid loss of molecules *via* this unknown mechanism made trapping impossible to observe. The inhomogeneous magnetic broadening was largely reduced to the underlying magnetic shift (as a function of the magnetic field in the trap region) by using a CCD camera to image the spatial distribution of the VO molecules. Moreover, because of the geometry of the trapping field and the probe beam, the fluorescence from the molecules at a given field strength (and hence the corresponding frequency shift) appears as a ring. Considerable information

about the g factors and hyperfine relaxation is gathered from this spatially resolved Zeeman spectroscopy.

This material is based upon work supported by the National Science Foundation under grant No. PHY-9511951. One of us (J.D.W.) is supported by a National Science Foundation Graduate Research Fellowship.

References

1 D. E. Pritchard, *Phys. Scr.*, 1995, **T59**, 131 and references therein.
2 N. Masuhara, J. M. Doyle, J. C. Sandberg, D. Kleppner, T. J. Greytak and H. F. Hess, *Phys. Rev. Lett.*, 1988, **61**, 935.
3 J. M. Doyle, B. Friedrich, J. Kim and D. Patterson, *Phys. Rev. A*, 1995, **52**, R2515.
4 J. Kim, B. Friedrich, D. Katz, D. Patterson, J. D. Weinstein, R. deCarvalho and J. M. Doyle, *Phys. Rev. Lett.*, 1997, **78**, 3665.
5 J. D. Weinstein, R. deCarvalho, J. Kim, D. P. Katz, D. Patterson, B. Friedrich and J. M. Doyle, *Phys. Rev. A*, 1998, **57**, R3173.
6 C. E. Moore, *Atomic energy levels*, Natl. Bur. Stand. Circ. No. NRDS-NBS35; U. S. GPO, Washington, DC, 1971.
7 W. C. Martin, R. Zalubas and L. Hagan, *Atomic energy levels—The rare earth elements*, Natl. Bur. Stand. Circ. No. NSRDS-NBS60; U. S. GPO, Washington, DC, 1978.
8 B. Friedrich, A. Slenczka and D. Herschbach, *Can. J. Phys.*, 1994, **72**, 897.
9 M. G. Kozlov and V. F. Ezhov, *Phys. Rev. A*, 1994, **49**, 4502.
10 E. A. Hinds and K. Sangster, *AIP Conf. Proc.*, 1993, **270**, 77.
11 B. E. Sauer, J. Wang and E. A. Hinds, *Bull. Am. Phys. Soc., Ser. II*, 1994, **39**, 1060.
12 B. N. Ashkinadzi, V. F. Ezhov, M. N. Groshev, V. V. Jaschuk, A. Yu. Khazov, V. A. Knjazkov, M. G. Kozlov, V. L. Riabov and M. A. Yugaldin, *Preprint from the Russian Academy of Sciences, St. Petersburg* 1994.
13 G. Timp, R. E. Behringer, D. M. Tennant, J. E. Cunningham, M. Prentiss and K. M. Berggren, *Phys. Rev. Lett.*, 1992, **69**, 1636.
14 R. E. Behringer, V. Natarajan and G. Timp, *Appl. Phys. Lett.*, 1996, **68**, 1034.
15 K. S. Johnson, K. K. Berggren, A. Black, C. T. Black, A. P. Chu, N. H. Dekker, D. C. Ralph, J. H. Thywissen, R. Younkin, M. Tinkhorn, M. Prentiss and G. M. Whitesides, *Appl. Phys. Lett.*, 1996, **69**, 2773.
16 D. W. Noid, S. K. Gray and S. A. Rice, *J. Chem. Phys.*, 1986, **84**, 2649.
17 S. K. Gray and S. A. Rice, *J. Chem. Phys.*, 1985, **83**, 2818.
18 J. T. Bahns, P. L. Gould and W. C. Stwalley, *J. Chem. Phys.*, 1996, **104**, 9689.
19 B. Friedrich and D. Herschbach, *Z. Phys. D*, 1991, **18**, 153.
20 B. Friedrich and D. Herschbach, *Nature* (*London*), 1991, **353**, 412.
21 B. Friedrich and D. Herschbach, *Z. Phys. D*, 1992, **24**, 25.
22 J. D. Miller, R. A. Cline and D. J. Heinzen, *Phys. Rev. A*, 1993, **47**, R4567.
23 W. D. Philips, in *Laser Manipulation of Atoms and Ions*, ed. E. Arimondo, W. Philips, and F. Sturmia, School of Atomic Physics "Enrico Fermi," Course CXVIII; North Holland, Amsterdam, 1992, pp. 334–335,
24 B. Friedrich and D. Herschbach, *Phys. Rev. Lett.*, 1995, **74**, 4623.
25 W. Ketterle and N. J. van Druten, *Adv. At. Mol. Opt. Phys.*, 1996, **37**, 181.
26 M. H. Anderson, J. R. Ensher, M. R. Matthews, C. E. Wieman and E. A. Cornell, *Science*, 1995, **269**, 198.
27 K. B. Davis, M.-O. Mewes, M. R. Andrews, N. J. van Druten, D. S. Durfee, D. M. Kurn and W. Ketterle, *Phys. Rev. Lett.*, 1995, **76**, 3969.
28 C. C. Bradley, C. A. Sackett and R. G. Hulet, *Phys. Rev. Lett.*, 1997, **78**, 985.
29 J. R. Heath, Q. L. Zhang, S. C. O'Brien, R. F. Curl, H. W. Kroto and R. E. Smalley, *J. Am. Chem. Soc.*, 1987, **109**, 359.
30 J. Wilks, in *The Properties of Liquid and Solid Helium*, Clarendon Press, Oxford, 1987. The vapor pressure of ^{4}He is determined from extrapolation of data in this reference.
31 *J. Res. Nat. Bureau of Stds.—A, Phys. Chem.* 1964, **68**, 579. Densities of ^{3}He gas are determined from extrapolation of data in this reference.
32 G. J. Zaal, W. Hogervorst, E. R. Eliel, K. A. H. van Leuwen and J. Blok, *Z. Phys. A*, 1979, **290**, 339.
33 *Experimental Transition Probabilities for Spectral Lines of Seventy Elements*, NBS53, US Department of Commerce, NBS, 1962.
34 K. B. Blagoev and V. A. Komarovskii, *At. Data Nucl. Data Tables*, 1994, **56**, 1.
35 N. A. Kuebler, M. B. Robin, J. J. Yang, A. Gedanken and D. R. Herrick, *Phys. Rev. A*, 1988, **38**, 737.
36 H. Herzberg, *Molecular Spectra and Molecular Structure. I. Spectra of Diatomic Molecules*, Van Nostrand Reinhold Company, New York, 1950.
37 K. P. Huber and G. Herzberg, *Molecular Spectra and Molecular Structure. IV. Constants of Diatomic Molecules*, Van Nostrand Reinhold Company, New York, 1979.
38 C. Townes and A. Schawlow, *Microwave Spectroscopy*, Dover, New York, 1975.
39 K. Ritter and T. Wilkerson, *J. Mol. Spectrosc.*, 1987, **121**, 1.
40 C. Naulin, M. Costes and G. Dorthe, *Chem. Phys.*, 1991, **153**, 519.
41 H. Zacharias, J. Halpern and K. Welge, *Chem. Phys. Lett.*, 1976, **43**, 41.
42 D. Jacobs, R. Madix and R. N. Zare, *J. Chem. Phys.*, 1986, **85**, 5469.
43 J. D. Weinstein, R. deCarvalho, K. Amar, A. Boca, B. C. Odom, B. Friedrich and J. M. Doyle, *J. Chem. Phys.*, submitted.
44 A. S.-C. Cheung, R. C. Hansen and A. J. Merer, *J. Mol. Spectrosc.*, 1982, **91**, 165.

Paper 7/08859K; *Received* 9*th December*, 1997